Chinese Chemical Letters 32 (2021) 2411–2414

Contents lists available at ScienceDirect

Chinese Chemical Letters

journal homepage: www.elsevier.com/locate/cclet

Communication

# Mild hyperthermia-enhanced chemo-photothermal synergistic therapy using doxorubicin-loaded gold nanovesicles

Zhuoting Deng[1], Chao Jiang[1], Muhammad Rizwan Younis, Shan Lei, Yaling He, Haoxing Zheng, Peng Huang, Jing Lin*

*Marshall Laboratory of Biomedical Engineering, International Cancer Center, Laboratory of Evolutionary Theranostics (LET), School of Biomedical Engineering, Shenzhen University Health Science Center, Shenzhen 518060, China*

ARTICLE INFO

*Article history:*
Received 14 December 2020
Received in revised form 29 March 2021
Accepted 30 March 2021
Available online 31 March 2021

*Keywords:*
Mild hyperthermia
Chemo-photothermal synergistic therapy
Gold nanovesicles
Doxorubicin
Photoacoustic imaging

ABSTRACT

Gold nanovesicles (GVs) with unique plasmonic property and large cavity hold great potential as a stimuli-responsive nanocarrier to deliver drugs for efficient tumor chemotherapy and other therapies synergistically. Herein, we developed doxorubicin-loaded gold nanovesicles (DGVs), offering infrared thermal (IRT) and photoacoustic (PA) dual-modal imaging guided mild hyperthermia-enhanced chemo-photothermal cancer synergistic therapy. The DGVs are self-assembled by gold nanoparticles modified with amphiphilic copolymer in a predetermined concentration of doxorubicin through film rehydration method. Under the influence of laser excitation, the as-prepared DGVs exhibited good photothermal effect, which triggered the structural disruption of GVs and thus, allowed the efficient release of encapsulated DOX to enhance cell uptake for fluorescence imaging and tumor chemotherapy, respectively. In addition, DGVs also showed a strong PA and IRT signals *in vivo*. Our study demonstrated the potential of DGVs as stimuli-responsive drug delivery systems and cancer theranostics.


Nanoparticle-based drug delivery systems (NDDSs) exhibit great potential to conquer the inherent limitations of conventional chemotherapy [1–11]. Exploiting the external physical stimuli such as light [12], heat [13,14], gas or internal tumor microenvironment like acidic. [15–17], a series of drug delivery carriers such as liposomes [18,19], polymeric micelles [20,21], mesoporous silica [22,23], and exosomes [24,25], were developed as stimuli-responsive NDDSs. However, these carriers usually suffered from drug leakage and low loading efficiency, which hinder their practical biomedical applications. Therefore, an ideal stimuli-responsive NDDS should overcome these issues. Additionally, conventional chemotherapy showed poor treatment efficiency and usually led to tumor regeneration or metastasis, owing to the development of multi-drug resistant cancer cells [26–28]. Therefore, the development of stimuli-responsive NDDSs with chemotherapy and other therapies synergistically is highly desirable for cancer treatment [29–31].

Gold nanovesicles (GVs) with unique plasmonic property and large cavity have attracted strong interest thanks to their light-responsive and excellent photothermal property [32,33], high drug loading capacity, good biocompatibility, and the effective prevention of drug leakage [34–37]. By taking an advantage of the enhanced plasmonic coupling effect, a number of GVs have been explored for biosensors [38,39], photothermal therapy (PTT) [40,41] and combinatorial/synergistic therapy [42–48]. Recently, mild hyperthermia-enhanced chemo-photothermal synergistic therapy is a newly developed strategy with a low drug and laser dose, offering remarkable cancer therapeutic effects due to the combined effect of PTT and chemotherapy [49–52].

Herein, we report a doxorubicin-loaded gold nanovesicles (DGVs) for infrared thermal (IRT), fluorescence and photoacoustic (PA) imaging guided mild hyperthermia enhanced chemo-photothermal synergistic therapy (Scheme 1). The DGVs are self-assembled by gold nanoparticles (AuNPs) coated with a biodegradable poly(ethylene glycol)-*b*-poly(ε-caprolactone) (PEG-*b*-PCL) block copolymer (denoted as AuNP-BCPs) in a predetermined concentration of doxorubicin (DOX) through film rehydration method. The as-prepared DGVs exhibit strong near-infrared (NIR) absorption and thus, demonstrate excellent PA signal and enhanced photothermal conversion efficiency (PCE, 35%) under NIR laser irradiation. The DGVs show drug loading capacity of ~15 wt%, while a controllable release of DOX is noticed under laser irradiation. Importantly, by integrating PTT with chemotherapy,

* Corresponding author.
*E-mail address:* jingl@szu.edu.cn (J. Lin).
[1] These authors contributed equally to this work.

https://doi.org/10.1016/j.cclet.2021.03.080
1001-8417/

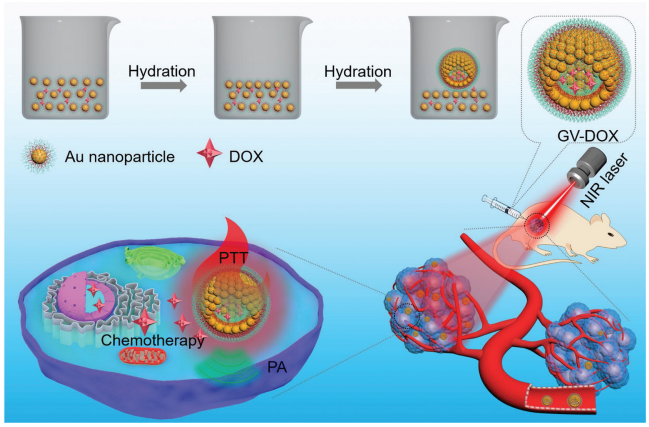


**Scheme 1.** Synthesis of doxorubicin-loaded gold nanovesicles (DGVs) through film rehydration method for mild hyperthermia enhanced chemo-photothermal synergistic therapy.

DGVs show complete tumor eradication in mice due to the synergistic chemo-photothermal therapeutic effect. Additionally, the DGVs with high PCE and strong NIR absorption hold great potential as a multimodal imaging contrast agent. These findings demonstrate the development of a multifunctional and stimuli-responsive NDDS for multimodal imaging guided mild hyperthermia-enhanced chemo-photothermal synergistic tumor therapy.

Firstly, AuNPs with 26 nm size (Fig. S1 in Supporting information) were prepared according to the reported method [53]. FmocNH-PEG-*b*-PCL-TE (*M*n = 25.9 kg/mol, PDI = 1.43) was synthesized by our previous reported method (Fig. S2 in Supporting information) and characterized in Fig. S3 (Supporting information) [41]. Next, GVs were self-assembled with the modified FmocNH-PEG-*b*-PCL-TE-tethered AuNPs through AuNPs film rehydration in water under sonication [54]. The as-prepared GVs exhibited interior cavity (Figs. 1a and b). The size of GVs was about 198 nm as determined by dynamic light scattering (DLS) measurement (Fig. S4 in Supporting information). Interestingly, as the assembly of AuNPs significantly shortened the distance between particles and the enhanced plasmonic coupling effect between adjacent AuNPs, the resultant GVs demonstrated red-shifted localized surface plasmon resonance band (Fig. 1c). The strong absorption in the range of 650−1000 nm indicated that GVs can be used as a PA/PTT agent.

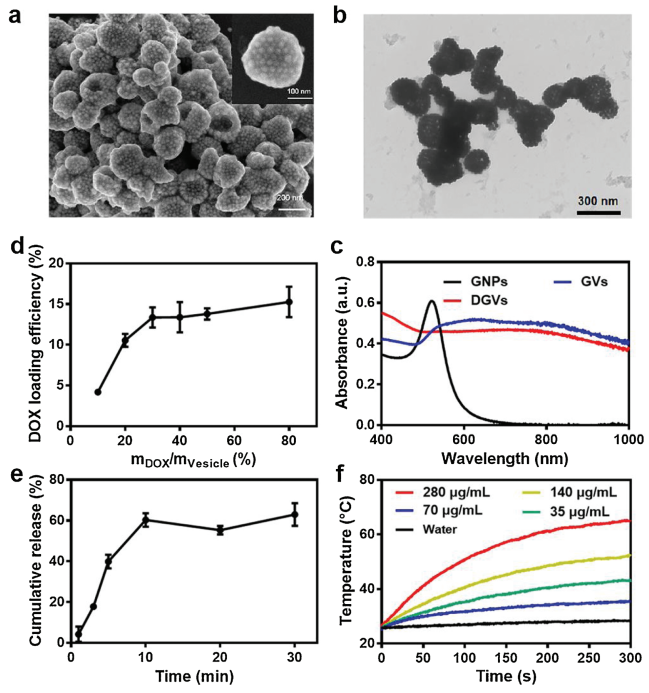


**Fig. 1.** (a) SEM and (b) TEM images of self-assembled GVs. (c) UV-vis-NIR absorption spectra of AuNPs, GVs and DGVs. (d) DOX loading efficiency of DGVs at different concentration of DOX. (e) DOX release profiles at different time and (f) DGVs concentration (0, 35, 70, 140 and 280 μg/mL) dependent temperature increase under laser irradiation (808 nm, 1.0 W/cm$^2$).

Next, DOX was encapsulated into the GVs. After DOX loading, the DGVs had no significant change of absorption compared to GVs (Fig. 1c), while their average size increased to 235 nm (Fig. S5 in Supporting information). Moreover, the fluorescence signal of DOX was detected in DGVs (Fig. S6 in Supporting information), suggesting the successful encapsulation of DOX by GVs. The loading efficiency of DOX by GVs was tested at different concentrations of DOX (Fig. 1d), calculated by standard curve method (Fig. S7 in Supporting information). It has been noticed the loading amount of DOX increases with the increase of DOX concentrations and reached a plateau at ~15%, when the weight ratio of DOX and GVs reached 80%. Next, the photothermal-triggered release of DOX from DGVs was investigated under 808 nm laser with different irradiation time (Fig. 1e). With the increase of irradiation time, the release of DOX gradually increased and reached a plateau about 61% at 10 min. In contrast, without laser irradiation, negligible release of DOX (less than 1%) was observed after incubation with PBS at pH 7.4, 6.5, or 5.5 for 24 h (Fig. S8 in Supporting information). These results suggested that the release of DOX in DGVs can be controlled by laser irradiation, due to the photothermal-triggered destruction/dissociation of GVs.

After that, the photothermal effect of DGVs was investigated. The control group (pure water) and a series of DGVs with different concentrations were irradiated with NIR laser (808 nm, 1.0 W/cm$^2$, 5 min). The temperature of DGVs solutions increased with the increase of the exposure time and concentration, while the water did not show any notable change in temperature (Fig. 1f). Similarly, under different laser powers, temperature increase (up to 65 °C) was noticed with the increase of laser densities from 0.1 W/cm$^2$ to 1.0 W/cm$^2$ (Fig. S9 in Supporting information). Hence, a significant temperature increase indicated the strong plasmonic coupling effect of DGVs, resulting the effective photothermal effect as well as light-activated drug release.

*In vitro* biocompatibility of DGVs was examined on HEK 293 T cells and U87-MG cells by MTT assay. As shown in Fig. 2a, both HEK 293 T and U87-MG cells had higher survival rates with increased dose of DGVs, confirming the good biocompatibility of DGVs. In addition, the cell cytotoxicity and *in vitro* chemo-photothermal synergistic therapy of DGVs were then evaluated (Fig. 2b). DGVs exhibited relatively low toxicity compared to pure DOX after incubation for 24 h in dark. However, under 808 nm laser irradiation (1.0 W/cm$^2$, 5 min), the viability of U87-MG cells decreased significantly with the concentration increase of DGVs, while a cell viability of less than 10% was observed at a concentration of 30 μg/mL (DOX concentration). The synergistic therapy exhibited obviously improved antitumor effects, compared with DOX induced chemotherapy or GVs-instructed PTT, which suggesting that the DGVs can achieve greater synergistic antitumor therapeutic effects than single treatment modality. The probable mechanism of synergistic effect was that DGVs generated mild hyperthermia under low dose of NIR laser irradiation, which can enhance the cellular uptake of DGVs and destruct the structure of DGVs to release more DOX within cells, thus achieving mild hyperthermia-enhanced chemo-photothermal synergistic therapy. Afterwards, the irradiation-enhanced cellular uptake of DGVs was investigated on U87-MG cells (Fig. 2c). As shown in Fig. 2d,

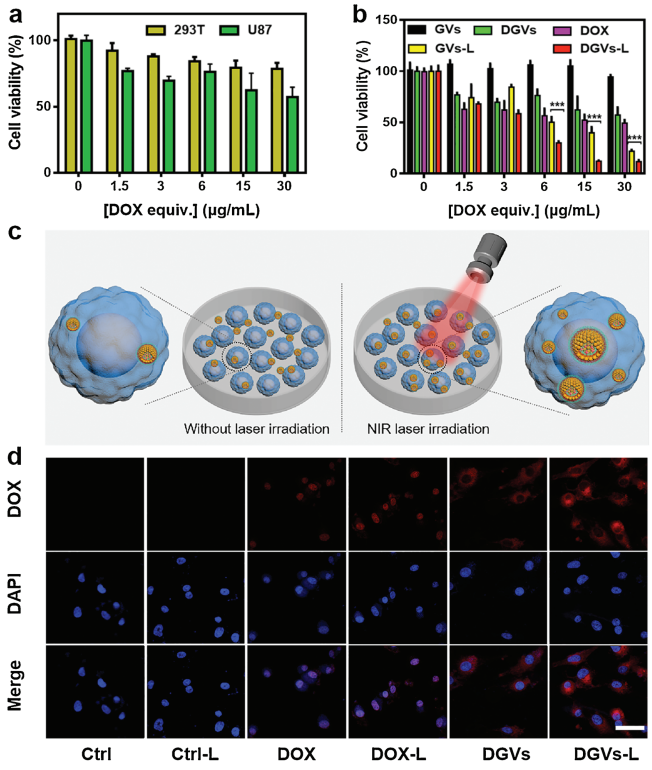


**Fig. 2.** (a) Concentration dependent cytotoxicity of the DGVs incubated with U87-MG and HEK 293 T cells in dark. (b) U87-MG cell viability after incubated with different concentrations of GVs, DOX, and DGVs for 4 h at 37 °C with/without 808 nm laser irradiation (1.0 W/cm$^2$) for 5 min. $^{***}P <$ 0.001. (c) Schematic illustrating the uptake of U87-MG cells with/without 808 nm laser irradiation. (d) Confocal fluorescence images analyses of U87-MG cells incubated with either free DOX or DGVs (DOX concentration: 30 μg/mL) with/without 808 nm laser irradiation (1.0 W/cm$^2$, 5 min). Scale bar: 25 μm.

U87-MG cells incubated with free DOX then treated with/without mild hyperthermia-NIR laser did not show any obvious difference in the fluorescence intensity of DOX. Whereas, NIR laser treated cells incubated with DGVs showed higher fluorescence intensity, suggesting mild hyperthermia could enhance the cellular uptake and drug release, simultaneously.

Encouraged by *in vitro* results, *in vivo* ITR/PA capacities of DGVs were investigated using U87-MG tumor-xenograft model. All animal experiments were approved by the Animal Ethics Committee of Shenzhen University and complied with all relevant policies and regulations. The mice received an intratumoral injection of DGVs (50 μL, corresponding to 40 μg/mL DOX) when tumor size reached about 60 mm$^3$. As shown in Fig. 3a, IRT images were recorded under 808 nm laser irradiation (0.5 W/cm$^2$, 10 min), the GVs and DGVs increased the local tumor temperature up to 47.5 °C and 48 °C, respectively (Fig. 3b), while no significant temperature was increased in PBS treated group. All these results demonstrated the DGVs could be a candidate as PTT agent. The PA property of DGVs was evaluated by PA imaging. DGVs exhibited strong concentration dependent PA signal enhancement (Figs. S10a and b in Supporting information). As shown in Fig. 3c, intense PA signals were observed in the tumor region, which was nearly 10-fold stronger than pre-injection (Figs. 3d and e).

The *in vivo* antitumor efficacy of DGVs was also conducted in same tumor-bearing mice model. Six groups (five mice per group) were set as follows: (i) Control, (ii) free DOX, (iii) GVs only, (iv) GVs-Laser, (v) DGVs only, and (vi) DGVs-Laser. Under different treatments, body weight of all groups had no obvious change within 14 days (Fig. S11 in Supporting information). For the laser groups (iv) and (vi), the tumor tissues were efficiently inhibited, suggesting the prominent antitumor effects. However, the tumors of other groups were found negligible growth inhibition. The tumors of DGVs-Laser treated group were wholly eliminated and no tumor regrew in 14 days observation (Fig. 4a). Appreciably, the DGVs-Laser treated group was tumor-free survival during 40 days neither death nor tumor recurrence. The GVs-Laser group had a little delay in the tumor growth and the others showed 14–35 days life spans (Fig. 4b). The frozen tumor sections were also prepared to analyze DOX distribution in tumor tissues. As shown in Fig. 4c, few red fluorescence of DOX was found in tumor treated with DGVs; while, an intense red fluorescence signal was observed in the tumor treated with DGVs-laser, which confirmed laser-irradiation induced mild hyperthermia could enhance tumor accumulation and active drug release in tumor tissues *in vivo*. As shown in Fig. 4d, hematoxylin and eosin (H&E) stained images of

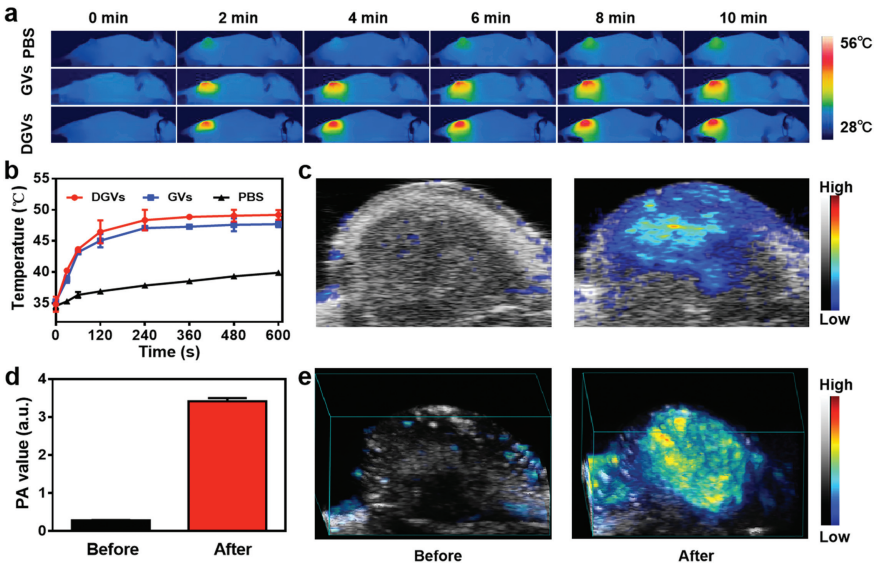


**Fig. 3.** (a) *In vivo* IRT images and (b) the corresponding temperature variations of the tumor region treated with PBS, GVs and DGVs exposed with NIR laser. (c) *In vivo* 2D images, (d) the corresponding intensities and 3D images (e) of PA in tumor region before and after injection of DGVs.

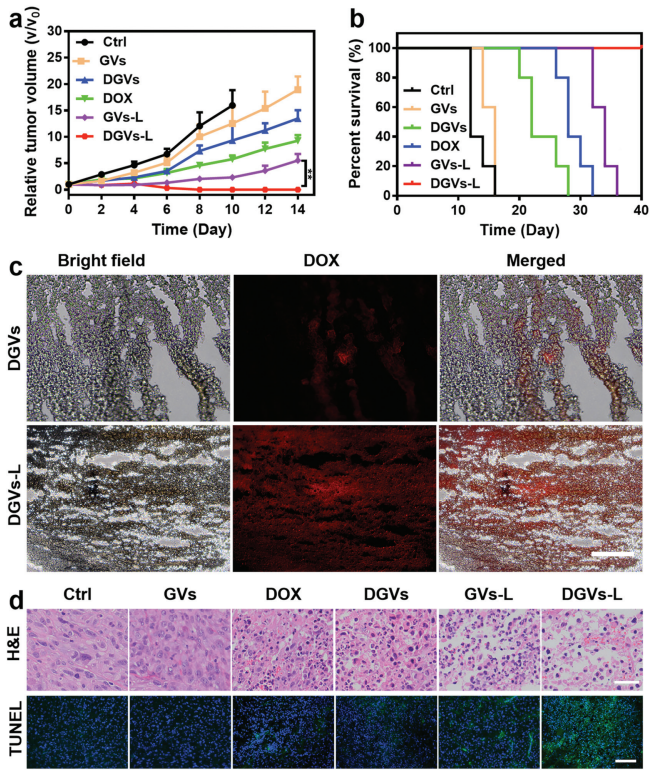


**Fig. 4.** (a) Tumor growth and (b) survival curves of tumor-bearing mice after different treatments. (mean ± SD, $n = 5$; $^{**}P < 0.01$). (c) Fluorescence images of frozen tumor sections after administration of DGVs with or without NIR laser. Scale bar: 200 μm. (d) H&E and TUNEL stained images of tumor sections. Scale bars are 50 and 200 μm, respectively.

tumor sections exhibited intensive necrosis area and pyknosis, whereas other groups showed infiltrating tumor cells with many mitoses. None of side effects like damage or inflammation was observed in major organs (Fig. S12 in Supporting information). The terminal deoxynucleotidyl transferase-mediated dUTP nick-end labeling (TUNEL) immunofluorescence assay showed the green fluorescence signal of mice treated with DGVs-Laser is strongest in all treated groups, suggesting DGVs-Laser treated group can induce most cell apoptosis (Fig. 4d). These results indicated that DGVs can achieve mild hyperthermia-enhanced chemo-photothermal cancer synergistic therapy *in vivo*.

In this work, we have developed a light-responsive drug delivery nanoplatform for IRT/PA dual-modal imaging guided mild hyperthermia-enhanced chemo-photothermal therapy. The strong NIR absorption of GVs and the payload of active compound such as DOX in GVs enable the mild hyperthermia-enhanced synergistic tumor therapy. The DGVs show high DOX loading efficiency, photothermal enhanced DOX uptake into cells, dual-modality imaging and synergistic chemo-photothermal treatment. Moreover, DGVs with high stability avoiding drug leakage could be facilitated to develop an excellent stimuli-responsive NDDS, thus overcoming the inherent limitations of chemotherapy and showing great potential for cancer theranostics.

## Declaration of competing interest

The authors report no declarations of interest.

## Acknowledgments

This work is financially supported by the National Natural Science Foundation of China (Nos. 31771036, 51703132), the Basic Research Program of Shenzhen (Nos. JCYJ20180507182413022, JCYJ20170412111100742), the Guangdong Province Natural Science Foundation of Major Basic Research and Cultivation Project (No. 2018B030308003). We thank Instrumental Analysis Center of Shenzhen University (Lihu Campus).

## Appendix A. Supplementary data

Supplementary material related to this article can be found, in the online version, at doi:https://doi.org/10.1016/j.cclet.2021.03.080.

## References

[1] M.K. Yu, Y.Y. Jeong, J. Park, et al., Angew. Chem. Int. Ed. 47 (2008) 5362–5365.
[2] S. Li, K. Hu, W. Cao, et al., Nanoscale 6 (2014) 13701–13709.
[3] J. Wen, K. Yang, F. Liu, et al., Chem. Soc. Rev. 46 (2017) 6024–6045.
[4] C. Zhu, D. Huo, Q. Chen, et al., Adv. Mater. 29 (2017) 1868–1872.
[5] Q. Zou, M. Abbas, L. Zhao, et al., J. Am. Chem. Soc. 139 (2017) 1921–1927.
[6] T. Liu, C. Wang, X. Gu, et al., Adv. Mater. 26 (2014) 3433–3440.
[7] K. Yang, L. Hu, X. Ma, et al., Adv. Mater. 24 (2012) 1868–1872.
[8] C. Chen, X. Ni, S. Jia, et al., Adv. Mater. 31 (2019) e1904914.
[9] C. Chen, X. Ni, H. Tian, et al., Angew. Chem. Int. Ed. 59 (2020) 10008–10012.
[10] C. Chen, H. Ou, R. Liu, D. Ding, Adv. Mater. 32 (2020) e1806331.
[11] X. Ni, X. Zhang, X. Duan, et al., Nano Lett. 19 (2019) 318–330.
[12] S. Yang, L. Zhou, Y. Su, et al., Chin. Chem. Lett. 30 (2019) 187–191.
[13] D. Zhang, J. Zhang, J. Zeng, et al., J. Biomed. Nanotechnol. 15 (2019) 288–300.
[14] Q. Huang, Y. Zou, S. Zhong, et al., J. Biomed. Nanotechnol. 15 (2019) 910–920.
[15] X. Li, Y. Zhang, Z. Ma, et al., Chin. Chem. Lett. 30 (2019) 489–493.
[16] J. Wang, K. Ma, H. Wang, et al., J. Biomed. Nanotechnol. 15 (2019) 2164–2178.
[17] Y. Qu, B. Chu, X. Wei, et al., J. Control. Release 296 (2019) 93–106.
[18] T. Fujimoto, M. Ito, S. Ito, H. Kanazawa, J. Biomater. Sci. Polym. Ed. 28 (2017) 679–689.
[19] E. Yuba, N. Tajima, Y. Yoshizaki, et al., Biomaterials 35 (2014) 3091–3101.
[20] C. Huang, C. Lo, H. Chen, G. Hsiue, Adv. Funct. Mater. 17 (2007) 2291–2297.
[21] Q. Zou, L. Zhang, X. Yan, et al., Angew. Chem. Int. Ed. 53 (2014) 2366–2370.
[22] X. Fang, X. Zhao, W. Fang, C. Chen, N. Zheng, Nanoscale 5 (2013) 2205–2218.
[23] W. Wu, C. Ye, H. Xiao, et al., Int. J. Pharm. 511 (2016) 65–72.
[24] P. Yang, S. Gai, J. Lin, Chem. Soc. Rev. 41 (2012) 3679–3698.
[25] L. Barile, G. Vassalli, Pharmacol. Ther. 174 (2017) 63–78.
[26] X. Xie, H. Nie, Y. Zhou, et al., Nat. Commun. 10 (2019) 5476–5490.
[27] J. Waaler, O. Machon, L. Tumova, et al., Cancer Res. 72 (2012) 2822–2832.
[28] D. Lu, M. Choi, J. Yu, et al., Proc. Natl. Acad. Sci. U. S. A. 108 (2011) 13253–13257.
[29] G. Szakacs, J.K. Paterson, J.A. Ludwig, C. Booth-Genthe, M.M. Gottesman, Nat. Rev. Drug Discov. 5 (2006) 219–234.
[30] G. Liu, J. Zou, Q. Tang, et al., ACS Appl. Mater. Interfaces 9 (2017) 40077–40086.
[31] R. Xing, K. Liu, T. Jiao, et al., Adv. Mater. 28 (2016) 3669–3676.
[32] B. Bezares, Y. Jaña, L. Cottet, A. Castillo, Mater. Express 8 (2018) 450–456.
[33] C. Salinas, E. Rodríguez-Sevilla, E. Flores-Romero, J.C. Cheang-Wong, Mater. Express 9 (2019) 141–149.
[34] J. Sun, Y. Guo, R. Xing, et al., Colloids Surf. A Physicochem. Eng. Aspects 514 (2017) 155–160.
[35] J. He, Y. Liu, T. Babu, Z. Wei, Z. Nie, J. Am. Chem. Soc. 134 (2012) 11342–11345.
[36] Y. Liu, J. He, K. Yang, et al., Angew. Chem. Int. Ed. 54 (2015) 15809–15812.
[37] J. He, Z. Wei, L. Wang, et al., Angew. Chem. Int. Ed. 52 (2013) 2463–2468.
[38] X. Huang, Y. Liu, J. Barr, et al., Nanoscale 10 (2018) 13202–13211.
[39] H. Ye, K. Yang, J. Tao, et al., ACS Nano 11 (2017) 2052–2059.
[40] Z. Yang, J. Song, Y. Dai, et al., Theranostics 7 (2017) 2177–2185.
[41] P. Huang, J. Lin, W. Li, et al., Angew. Chem. Int. Ed. 52 (2013) 13958–13964.
[42] J. Song, L. Pu, J. Zhou, B. Duan, H. Duan, ACS Nano 7 (2013) 9947–9960.
[43] J. Lin, S. Wang, P. Huang, et al., ACS Nano 7 (2013) 5320–5329.
[44] J. Song, L. Pu, J. Zhou, H. Duan, ACS Nano 7 (2013) 9947–9960.
[45] K. Niikura, N. Iyo, Y. Matsuo, H. Mitomo, K. Ijiro, ACS Appl. Mater. Interfaces 5 (2013) 3900–3907.
[46] J. Song, Z. Fang, C. Wang, et al., Nanoscale 5 (2013) 5816–5824.
[47] J. Song, J. Zhou, H. Duan, J. Am. Chem. Soc. 134 (2012) 13458–13469.
[48] K. Zhu, G. Liu, G. Zhang, J. Hu, S. Liu, Macromolecules 51 (2018) 8530–8538.
[49] D.K. Kirui, C. Celia, R. Molinaro, et al., Adv. Healthc. Mater. 4 (2015) 1092–1103.
[50] N. Lu, P. Huang, W.P. Fan, et al., Biomaterials 126 (2017) 39–48.
[51] T. Feng, L. Zhou, Z. Wang, et al., Biomaterials 232 (2020) 119709.
[52] S. Wang, J. Weng, X. Fu, et al., Nanotheranostics 1 (2017) 208–216.
[53] Y. Liu, Y.J. Liu, J. Yin, Z. Nie, Macromol. Rapid Commun. 36 (2015) 711–725.
[54] A. Choucair, P.L. Soo, A. Eisenberg, Langmuir 21 (2005) 9308–9313.